Published in IET Microwaves, Antennas & Propagation
Received on 28th July 2009
Revised on 18th January 2010
doi: 10.1049/iet-map.2009.0399

ISSN 1751-8725

Construction of Green's functions of parallel plates with periodic texture with application to gap waveguides – a plane-wave spectral-domain approach

M. Bosiljevac[1] *Z. Sipus*[1] *P.-S. Kildal*[2]

[1]*Faculty of Electrical Engineering and Computing, University of Zagreb, Unska 3, Zagreb, Croatia*
[2]*Department of Signals and Systems, Chalmers University of Technology, Gothenburg, Sweden*
E-mail: marko.bosiljevac@fer.hr

Abstract: This study presents Green's functions of parallel-plate structures, where one plate has a smooth conducting surface and the other an artificial surface realised by a one-dimensional or two-dimensional periodic metamaterial-type texture. The purpose of the periodic texture is to provide cut-off of the lowest order parallel-plate modes, thereby forcing electromagnetic energy to follow conducting ridges or strips, that is, to form a gap waveguide as recently introduced. The Green's functions are constructed by using the appropriate homogenised ideal or asymptotic boundary conditions in the plane-wave spectral domain, thereby avoiding the complexity of the Floquet-mode expansions. In the special case of a single ridge or strip, an additional numerical search for propagation constants is needed and performed in order to satisfy the boundary condition on the considered ridge or strip in the spatial domain. The results reveal the dispersion characteristics of the quasi-transverse electromagnetic modes that propagate along the ridges or strips, including their lower and upper cut-off frequencies, as well as the theoretical decay of the modal field in the transverse cut-off direction. This lateral decay shows values of 50–100 dB per wavelength for realisable geometries, indicating that the gap waveguide modes are extremely confined. The analytical formulas for the location of the stopband of the lowest order parallel-plate modes obtained by small-argument approximation of the dispersion equation are also shown. To verify the proposed analysis approach, the results are compared with the results obtained with a general electromagnetic solver showing very good agreement.

1 Introduction

For exploring higher microwave frequencies, existing transmission line technologies are found to be either too expensive to manufacture or too lossy. This has triggered interest in the development of novel transmission lines and waveguides, such as the recently proposed metamaterial-based gap waveguide [1]. This has the potential of becoming an attractive solution for microwave applications above 30 GHz.

The essential idea of the gap waveguide is to use a periodic metamaterial-type loading of one of two parallel conducting surfaces in such a way that the lowest order parallel-plate modes are in cut-off, and thereby to force the waves to propagate in desired directions along the ridges or strips within the gap between the surfaces (see Fig. 1). There are two principally different types of gap waveguides that need different theoretical treatments (Fig. 1). We choose to refer to them as:

1. One-dimensional (1D) periodic type.

2. Two-dimensional (2D) periodic type.

The 1D periodic type is characterised by a purely 1D periodic texture in the lower surface that supports confined

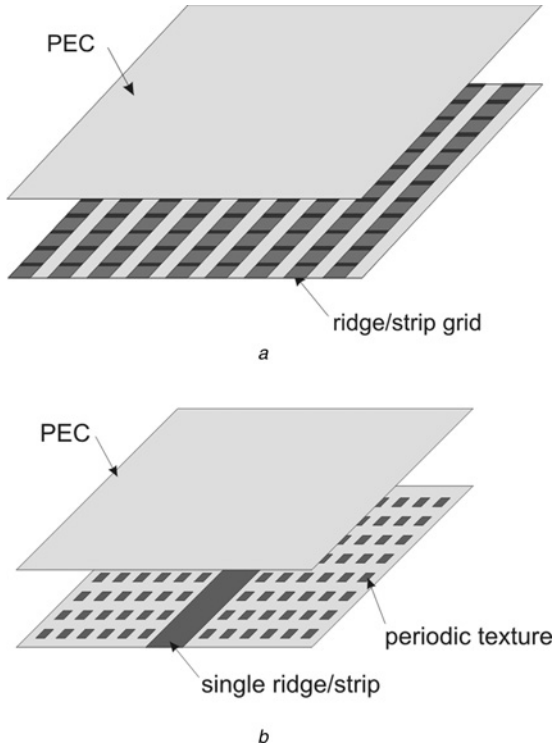

Figure 1 *Two gap waveguide types considered in the present paper*

a 1D periodic type allowing wave propagation along each single ridge or strip
b 2D periodic type with a 2D periodic texture in one plate allowing wave propagation only along the ridge or strip

local-mode wave propagation along parallel ridges or strips. The 2D periodic type has a 2D periodic artificial surface providing the parallel-plate cut-off and an additional single ridge or strip, along which confined local waves can propagate.

The ideal form of the latter 2D periodic-type structure comprises parallel perfect electric conductor (PEC) and perfect magnetic conductor (PMC) surfaces, and it exhibits cut-off if the spacing between the two surfaces, referred to as the gap height, is smaller than a quarter wavelength. Such a parallel-plate cut-off condition can be easily realised by using electromagnetic bandgap (EBG) surfaces, or high impedance surfaces (i.e. artificial magnetic conductors). The most common practical realisation of EBG surfaces is the so-called mushroom surface using periodic patches on a grounded substrate with vias [2], whereas here we use the pin surface (also called bed-of-nails) [3] because it is simpler to realise at high frequency when the dimensions are small.

The 1D periodic-type waveguide is based on the soft and hard surfaces concept [4], which allows wave propagation only in the hard direction. Ideally, the soft and hard surfaces are grids of parallel PEC and PMC strips and are most simply realised by corrugations, but they can also be realised by metal strips with vias [5]. The gap waveguide can also be understood as a miniaturised rectangular hard waveguide having two PEC walls and two PMC walls [6], where the vertical PMC walls are realised by the cut-off between two parallel plates, which gives a very wideband solution compared to the narrow-band frequency selective surface wall realisation in [6], and also compared to the simpler realisation using dielectrically loaded vertical walls.

The gap waveguide is a result of studies of parallel-plate waveguides in which one of the surfaces was loaded with longitudinal corrugations to provide a hard surface [7, 8]. The intention was to feed a planar slot array in a simple manner without having to locate several rectangular waveguides side-by-side. Feeding using one wide oversized rectangular waveguide caused problems with multiple modes, but these modes were successfully suppressed using a longitudinally corrugated hard surface. In addition, simulations in [7, 8] revealed uncoupled local waves following individual ridges between the corrugations which opened up the additional possibility of phase-steering in the plane transverse to the corrugations. These local waves were studied in detail in [9], and it finally resulted in the generalisation to the gap waveguide concept [1].

It is clear that gap waveguides have many potential applications (apart from building the feeding network for slot arrays). We will not discuss these here, but instead refer to [1, 10], where the latter describes cavity mode suppression when microstrip circuits are packaged in metal boxes. Thereby, the gap waveguide technology becomes a new and useful packaging technology for both passive and active microwave circuits, including also complete chips with MMICs.

The present paper will show how to derive the Green's functions of gap waveguides realised using different artificial surfaces described above. In particular, in Section 3, we shall deal with 1D types of periodic surfaces (ideal PEC/PMC grid and corrugated surface), and in Section 4 with 2D types of periodic surfaces (ideal PMC and bed-of-nails surface).The parallel-plate cut-off bandwidths of several artificial surfaces have already been investigated numerically in [11] by using a general electromagnetic solver, but here we will show how the dispersion equations and the whole Green's functions can be determined by using a more physical approach involving homogenised surface impedance formulations in the plane-wave spectral domain (all being explained for the general 1D and 2D periodic surface types in Section 2). This includes special treatment of the 2D periodic type due to the presence of the single and therefore non-periodic guiding ridge or strip.

It is important to be aware that the cut-off bandwidth (i.e. stopband of the lowest order parallel-plate modes) determines the useful bandwidth of the gap waveguide [1], or rather the potentially useful bandwidth, as there may be higher order gap waveguide modes present within this bandwidth if the strip or ridge is wide enough. Notice also that the cut-off bandwidth of the lowest-order parallel-plate modes has limited relation to the bandgap of surface

doi: 10.1049/iet-map.2009.0399

waves in the open periodically loaded surface. This can be seen by comparing the cut-off bandwidths in [11] with the surface wave bandgaps of the same open surfaces in [12], from which it can be seen that the lower cut-off frequency is approximately the same as the start frequency of the bandgap, whereas the upper cut-off frequency is very different from the stop frequency of the bandgap of the surface waves in the open surface.

Finally, it needs to be pointed out that the present results have been validated by using the general electromagnetic solver computer simulation technology (CST) Microwave Studio [13]. Microwave devices based on gap waveguides can of course always be analysed and designed by such general codes. However, the computer time will increase with the size of the devices in terms of wavelength. Therefore it is always of importance to derive faster analysis approaches such as the method of moments (MoM), and the first step in developing a moment method analysis approach is to find the Green's function of the analysed structure, which thereby motivates the present paper. The analytical treatment involved also improves the physical understanding of how the gap waveguide works, and therefore it can also help to improve the performance in the long run.

2 Homogenised plane-wave spectral-domain approach

2.1 Plane-wave spectral-domain approach

The derivation of the Green's functions will be obtained in the plane-wave spectral domain. The method was previously used commonly in the analysis of microstrip circuits and antennas, see for example, [14–17], where [17] represents the formulation and algorithm implementation of it used in the present paper. The plane-wave spectral domain is defined by

$$\tilde{\boldsymbol{E}}(k_x, k_y, z) = \int_{-\infty}^{\infty}\int_{-\infty}^{\infty} \boldsymbol{E}(x, y, z) e^{jk_x x} e^{jk_y y} \mathrm{d}x\,\mathrm{d}y \quad (1)$$

where '$\sim$' denotes the two-dimensional Fourier transformation with k_x and k_y the spectral variables, and correspondingly for the H-field. The spatially varying field is obtained by the corresponding inverse transformation.

Field solutions in the spectral domain (without single separate ridges or strips) can be determined by using the approach described in any of the references [14–17]. In short, we assume that the spectral solutions of the Helmholtz differential equation for E_z and H_z components of the electromagnetic field have the form

$$\tilde{E}_z(k_x, k_y, z) = A\cos(k_z z) + B\sin(k_z z) \quad (2a)$$

$$\tilde{H}_z(k_x, k_y, z) = C\cos(k_z z) + D\sin(k_z z) \quad (2b)$$

where the $e^{-jk_x x} e^{-jk_y y}$ variation is understood and suppressed. $k_z = \sqrt{k_0^2 - k_x^2 - k_y^2}$, k_0 is the free-space wavenumber and A, B, C and D are the unknowns which are determined by fulfilling the boundary conditions on each of the two surfaces for the x- and y-components of the fields. It is important to mention that it is sufficient to determine only the z-components of the electromagnetic field, whereas all the other components are given from these by (12) in [14].

2.2 Homogenisation using spectral surface admittance

The rigorous analysis of periodic structures can be performed by expanding the electromagnetic field into Floquet modes and then by using some general numerical approach (e.g. MoM, finite-element method (FEM) or finite-difference time-domain (FDTD)) to determine the fields and/or currents in a unit cell, but still this is very time consuming if the source excites a spectrum of plane waves, such as it does in our Green's function case (i.e. when we have a point source). However, it is possible to be much more computationally efficient by introducing some simplifications into the rigorous analysis approach, by which all electromagnetic effects will still be included.

The general idea is to use some approximate boundary condition replacing the periodic texture in the plane-wave spectral domain, and to derive the Green's functions for this simpler waveguide. We will assume that the period of the surface is very small compared to wavelength that will allow us to base the analysis on the so-called asymptotic boundary conditions [18]. In principle, the asymptotic boundary conditions are valid in the limit when the periodicity of the surface approaches zero. This homogenises the surface and captures the main physical phenomena. For example, it is isotropic for the 2D style periodic surface and anisotropic for the 1D periodic type.

The asymptotic boundary condition for the considered surface will be conveniently represented by the homogenised surface impedance in the plane-wave spectral domain. This will then have an angle of incidence variation (spectral k_x and k_y variation), through which the depth d of the surface is accounted for, and in general, we need to allow the surface impedance to be anisotropic. Further, it is advantageous to use the spectral surface admittance instead of the surface impedance, in order to avoid problems with the infinite impedance of PMC. Thus, we will finally use the general surface admittance components $\tilde{Y}_{xy}$ and $\tilde{Y}_{yx}$ defined by (the periodic surface coincides with the xy-plane)

$$\tilde{Y}_{yx} = \frac{\tilde{H}_y}{\tilde{E}_x}, \quad \tilde{Y}_{xy} = -\frac{\tilde{H}_x}{\tilde{E}_y} \quad (3)$$

doi: 10.1049/iet-map.2009.0399

2.3 Inverse transformation by contour integration in complex plane

The inverse Fourier transformation is not straightforward, because the desired modal solutions are represented by singularities in the spectral-domain expressions for the field. However, by changing the contour of integration in the complex $k_x k_y$ plane, it is possible to avoid numerical difficulties caused by the presence of the poles. In the case of PEC/PMC strips and corrugations, the poles are located on two lines [18, 19], and therefore the approach from [20] is adopted. In the case of the bed-of-nails structure, the poles are located on concentric circles and we have applied the integration in the polar coordinate system [21].

For the 1D periodic type, the analysis is completed by the inverse transformation, whereas for the 2D periodic type, we need to account for the boundary condition on the single non-periodic ridge or strip.

2.4 Single ridge/strip boundary condition

The ridge/strip itself is for the 2D surface type introduced into the analysis via an infinite transmission line current with propagation constant k_{eff} that is evaluated by using the approach described in [22]. This approach is as follows. The transmission line current is approximated as a travelling wave current of the form $J_y(x')e^{-jk_{\text{eff}}y'}$, where k_{eff} is the unknown propagation constant, y' is the position at the ridge or strip and $J_y(x')$ is an assumed expression for the transverse distribution across the ridge or strip of the longitudinal current. Thus, we assume that the current is entirely longitudinal, with a known current distribution. The simplest assumption for $J_y(x')$ is to assume that it is constant over the width, but it will give better results if the known singularities of the current at the sharp strip edges or 90° ridge wedges are included in $J_y(x')$ [23], see also Section 4.3. These assumptions on the travelling wave current may not be ideally correct for the ridge, in which case we may expect some transverse current components that continue down on both sides of the ridge, and not even for a wide strip, in which case we may also expect transverse current components. Still, we will use these approximations in the present work and study their accuracy by comparison with the numerical CST solution. An alternative would have been to compute the current distribution by expanding it in terms of several known functions (i.e. basis functions) with unknown coefficients, and solve for these coefficients using the MoM.

By transforming $J_y(x')$ to the spectral domain and inserting it into the inverse transform for the y-directed electric field, it is possible to find the field on the ridge itself. Enforcing the boundary condition that the $J_y(x')$-weighted electric field is zero across the ridge (this corresponds to the Galerkin's method when applying the MoM), the following characteristic equation is finally obtained

$$\int_{-\infty}^{\infty} \tilde{\tilde{G}}_{yy}^{\text{EJ}}(k_{\text{eff}}, k_x) \cdot \tilde{J}_y^2(k_x) \cdot \mathrm{d}k_x = 0 \tag{4}$$

Here $\tilde{\tilde{G}}_{yy}^{\text{EJ}}(k_{\text{eff}}, k_x)$ is the spectral domain Green's function for a y-directed source located just above the periodic texture in our waveguide. $\tilde{J}_y(k_x)$ is the Fourier transform of $J_y(x)$. From this equation it is possible to determine the propagation constant k_{eff} of the ridge current, and thereafter we can evaluate the modal field of the 2D periodic-type gap waveguide.

3 1D periodic-type structure

3.1 Ideal PEC/PMC strip grids

Let us first consider the ideal case where the lower surface consists of PEC and PMC strips with a period much smaller than the wavelength. The source is assumed to be a vertical (z-directed) electric source located just below the upper plate, as shown in Fig. 2.

The boundary conditions for this geometry are

$$\tilde{E}_y = 0, \quad \tilde{H}_y = 0, \quad \text{at } z = 0 \tag{5a}$$

$$\tilde{E}_x = \tilde{M}_y, \quad E_y = -\tilde{M}_x \quad \text{at } z = h \tag{5b}$$

The first two boundary conditions are actually the asymptotic boundary conditions for the PEC/PMC strips [18, 19]. M_x and M_y are horizontal magnetic replacement currents, which can be expressed using our actual vertical (z-directed) electric current source J_z by using (5) from Section 2.2 in [24]

$$\tilde{M}_x = \frac{k_y}{k_0/\eta_0}\tilde{J}_z, \quad \tilde{M}_y = -\frac{k_x}{k_0/\eta_0}\tilde{J}_z \tag{6}$$

where η_0 is the free-space impedance.

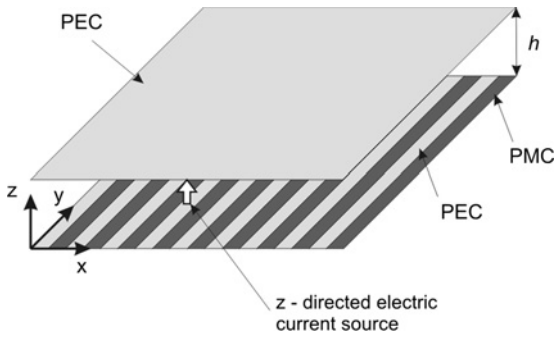

Figure 2 *Electric current source between parallel plates in which the lower plate is a PEC/PMC strip grid, that is, an ideal soft and hard surface*

doi: 10.1049/iet-map.2009.0399

Finally, we obtain the following expressions for the $\tilde{H}_x$ and $\tilde{H}_y$ fields, which are the main fields of interest in our case

$$\tilde{\tilde{G}}_{xz}^{\mathrm{HJ}} = \tilde{H}_x = j\frac{k_y}{k_0^2 - k_y^2}\left[-\frac{k_x^2}{k_z}\frac{\sin(k_z z)}{\cos(k_z h)} + k_z\frac{\cos(k_z z)}{\sin(k_z h)}\right] \quad (7a)$$

$$\tilde{\tilde{G}}_{yz}^{\mathrm{HJ}} = \tilde{H}_y = j\frac{1}{k_0^2 - k_y^2}\left[(k_0^2 - k_y^2)\frac{k_x}{k_z}\frac{\sin(k_z z)}{\cos(k_z h)}\right] \quad (7b)$$

The poles of the spectral-domain Green's functions correspond to propagation constants of waveguide modes. From these expressions, we notice that there exist classical global-type parallel-plate modes determined by the nulls of the functions $\cos(k_z h) = 0$ and $\sin(k_z h) = 0$. Furthermore, we have an additional guiding mode defined by $k_0^2 - k_y^2 = 0$. The latter is a so-called grating wave or strip wave that propagates along the strips. We have evaluated the transverse field variation as explained after (1). The result is depicted in Fig. 3, showing the x-component of the magnetic field just below the upper plate for a gap height of 3.5 mm and a frequency of 10 GHz. We understand from the graph that the fields that propagate in this mode follow the strips, and that they are strongly confined to the strips that are located directly below the source (the rate of the field decay is more than 100 dB/λ), thus effectively forming a narrow transmission line within the oversized waveguide (the figure shows the H-field distribution just below the upper PEC surface both for $y = 1\lambda_0$ and for $y = 5\lambda_0$). This is in spite of the fact that the source radiates omnidirectionally, and that it is located just below the upper waveguide plate (i.e. the PEC plane). Note that the field does not decay with the distance from the source, and thereby we have obtained a narrow confined transmission line mode within the parallel-plate waveguide.

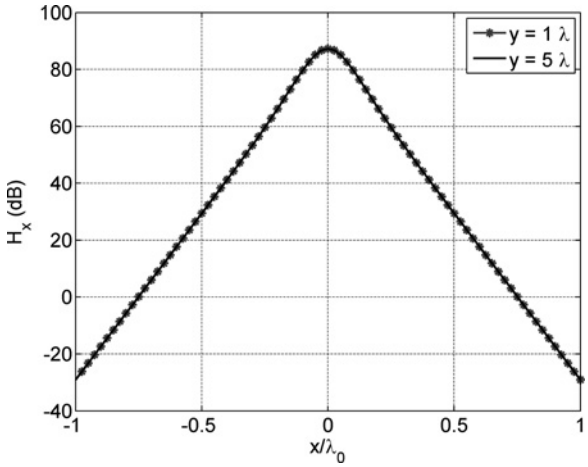

Figure 3 *H_x field evaluated at the upper surface in a plane transverse to the strip direction at two distances 1λ and 5λ away from the z-directed electric current source*

The produced confinement is a consequence of the fact that the characteristic equation $k_0^2 - k_y^2 = 0$ does not depend on the k_x value. A simple explanation for this behaviour lies in the property of the PEC/PMC strips, which in the x-direction behave as a soft surface and prevent the propagation of waves, whereas in the y-direction they act as a hard surface and therefore support wave propagation.

3.2 Corrugations

The same approach can be repeated for a practical case in which the PEC/PMC strips are realised as a corrugated surface as shown in Fig. 4. The properties of the corrugations are described using a spectral surface admittance $\tilde{Y}_{yx}$ defined as

$$\tilde{Y}_{yx} = \frac{\tilde{H}_y^{\mathrm{corr}}}{\tilde{E}_x^{\mathrm{corr}}} = j\frac{1}{k_0\eta_0}\frac{P}{W}\sqrt{\varepsilon_r k_0^2 - k_y^2}\cot\left(d\sqrt{\varepsilon_r k_0^2 - k_y^2}\right) \quad (8)$$

where ε_r is the permittivity of the medium inside the corrugations and d is the height of the corrugations. P and W represent the period and the width of the corrugations, respectively. This expression is derived in [19] with the assumption that the period of the corrugations is much smaller than the operating wavelength [18]. The following expressions for the $\tilde{H}_x$ and $\tilde{H}_y$ fields can be obtained

$$\tilde{\tilde{G}}_{xz}^{\mathrm{HJ}} = j\frac{k_y}{D_{\mathrm{SW}}}\left[-\frac{k_x^2}{k_z}\frac{\sin(k_z z)}{\cos(k_z h)} + k_z\frac{\cos(k_z z)}{\sin(k_z h)} - jk_0\eta_0\tilde{Y}_{yx}\frac{\cos(k_z z)}{\cos(k_z h)}\right] \quad (9a)$$

$$\tilde{\tilde{G}}_{yz}^{\mathrm{HJ}} = j\frac{1}{D_{\mathrm{SW}}}\left[(k_0^2 - k_y^2)\frac{k_x}{k_z}\frac{\sin(k_z z)}{\cos(k_z h)} + jk_0\eta_0 k_x\tilde{Y}_{yx}\frac{\cos(k_z z)}{\cos(k_z h)}\right] \quad (9b)$$

where D_{SW} is defined as

$$D_{\mathrm{SW}} = k_0^2 - k_y^2 - jk_0\eta_0 k_z\tilde{Y}_{yx}\tan(k_z h) \quad (10)$$

Apart from the classical global-type parallel-plate modes, like in the ideal PEC/PMC strip grid case, we again have a local confined gap wave that follows the corrugations, defined by

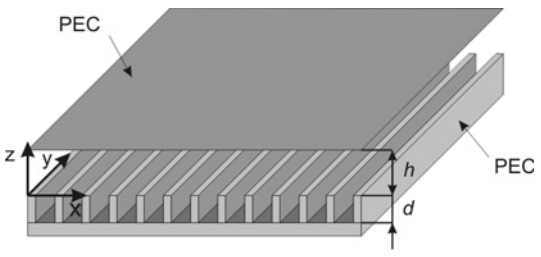

Figure 4 *Parallel-plate waveguide with one plate replaced by longitudinal corrugations*

$D_{SW} = 0$, that is, by

$$k_0^2 - k_y^2 - jk_0\eta_0 k_z \tilde{Y}_{yx} \tan(k_z h) = 0 \quad (11)$$

As an example, let us consider a waveguide that is designed to work in the frequency band around 10 GHz. The gap height of the considered waveguide is 3.5 mm. The corrugations are filled with dielectric material having permittivity $\varepsilon_r = 4.0$, the width of corrugations is 1.7 mm and the period is 2 mm ($W/P = 0.85$). This means that the depth of the corrugations is 4.33 mm, being defined by the so-called hard boundary condition

$$d = \frac{\lambda_0}{4\sqrt{\varepsilon_r - 1}} \quad (12)$$

The dispersion diagram for this case is computed by the present approach and presented in Fig. 5. It is computed for the soft x-direction for which there should be no wave propagation. The desired cut-off band can be observed between 8.66 and 10.85 GHz. The dispersion diagram computed using CST Microwave Studio [13] is also shown and confirms the results obtained by the present approach. It can be observed in [18] that the surface wave bandgap of the open corrugated surface ranges from 8.66 to 17.32 GHz (i.e. from f_{SOFT} to $2f_{SOFT}$), which is a much larger stop bandwidth than the cut-off bandwidth of the parallel-plates. This can be explained by taking a closer look at (9) for the soft direction ($k_y = 0$). By combining (8) and (11), the following is obtained

$$k_0^2 + \sqrt{\varepsilon_r} k_0 \frac{P}{W} \cot\left(\sqrt{\varepsilon_r} k_0 d\right) \cdot k_z \tan(k_z h) = 0 \quad (13)$$

Using a small argument approximation and the fact that at the cut-off frequency $k_z = k_0$, the characteristic equation in (11) can be reduced to the following approximate form

$$\lambda_{cut-off}^2 + \pi^2 h\sqrt{\varepsilon_r}\frac{P}{W} \cdot \lambda_{cut-off} - 4\pi^2 \varepsilon_r d h \frac{P}{W} = 0 \quad (14)$$

which gives the following upper cut-off wavelength

$$\lambda_{cut-off} = \frac{1}{2}\pi^2 \cdot h \cdot \sqrt{\varepsilon_r} \cdot \frac{P}{W} \cdot \left[-1 + \sqrt{1 + \frac{16}{\pi^2}\frac{d}{h}\frac{W}{P}}\right] \quad (15)$$

This gives for the present example an upper cut-off frequency at 11.45 GHz, compared to a numerically computed value of 10.85 GHz.

The complete dispersion diagrams have been determined by the present plane-wave approach for different dimensions of the corrugated surface, different gap heights and different permittivity in the grooves. The results are plotted in Fig. 6, showing both the lower and higher

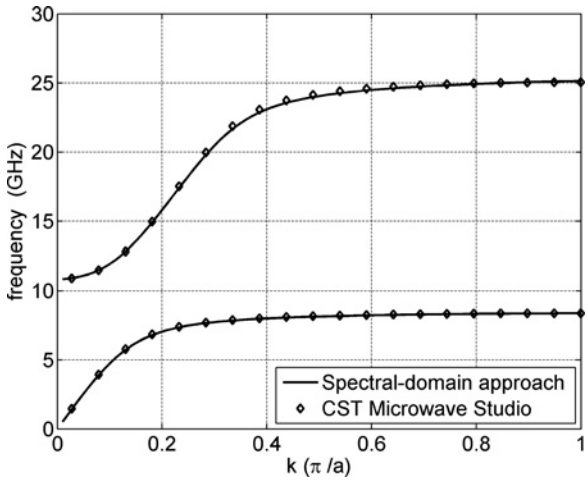

Figure 5 *Dispersion diagram for the parallel-plate waveguide with corrugations obtained for the soft direction (x)*

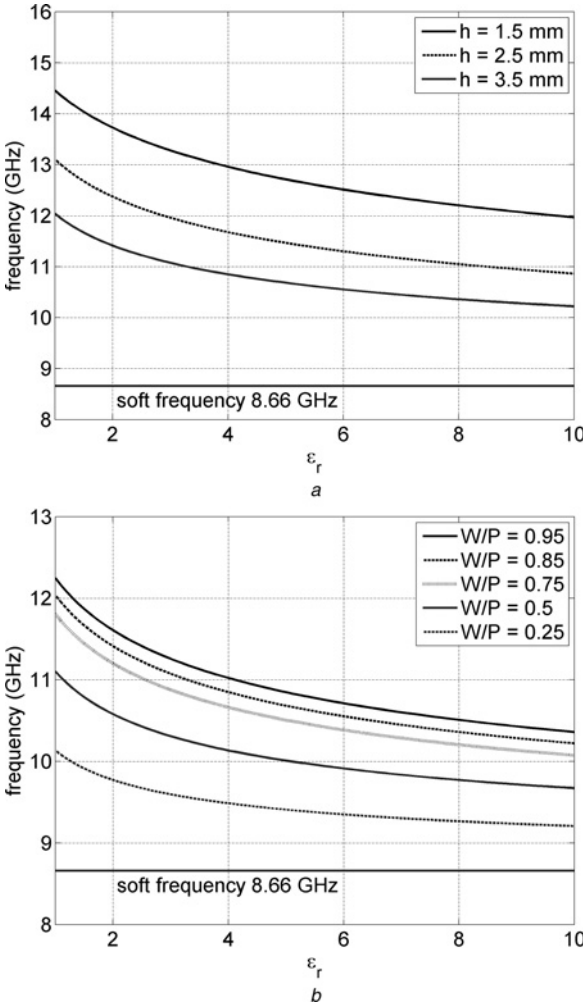

Figure 6 *Lower and upper cut-off frequencies for the parallel-plate waveguide with one corrugated surface for different dimensions and permittivities*

Lower cut-off frequency is approximately equal to the soft frequency

doi: 10.1049/iet-map.2009.0399

cut-off frequencies. The soft frequency (i.e. the approximate lower cut-off frequency) was fixed by appropriately selecting the depth d and permittivity ε_r of the corrugations $(d = \lambda_{soft}/4\sqrt{\varepsilon_r})$, whereas the upper cut-off frequency was determined by computation. The diagrams show how the dimensions and permittivity can be changed in order to obtain a reasonable bandwidth. In other words, by selecting a smaller height for the waveguide gap and a larger W/P ratio, it is possible to enlarge the cut-off bandwidth.

The transverse field distributions in the soft direction perpendicular to the corrugations and in the hard direction along the corrugations were computed using the spectral-domain approach when excited by a vertical short dipole located below the upper waveguide plate (i.e. below the PEC plate), and are presented in various ways in Figs. 7–9

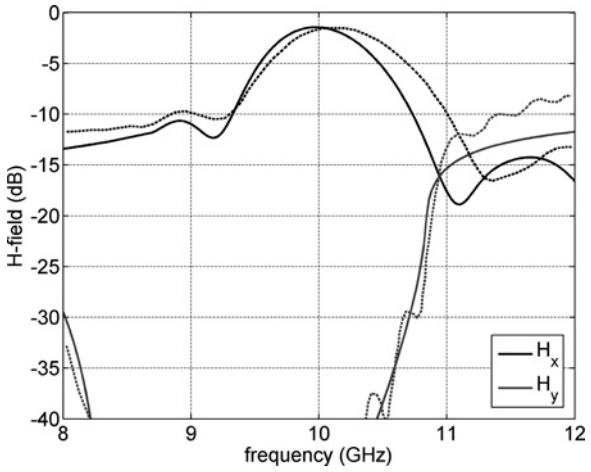

Figure 7 *Plot of the transversal magnetic fields H_x and H_y for the parallel-plate waveguide with corrugated surface obtained by the spectral-domain approach (solid lines) and by CST Microwave Studio (dashed lines)*

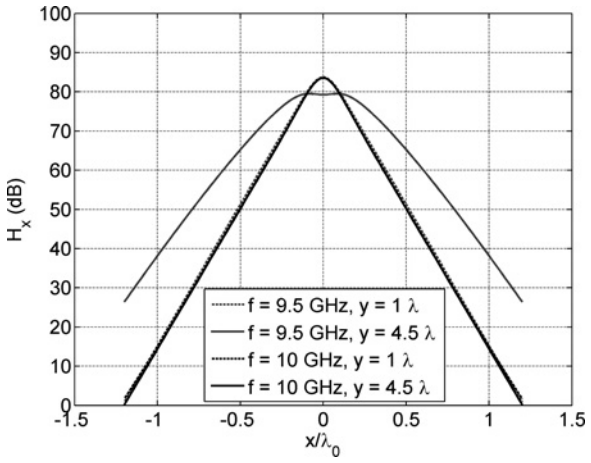

Figure 8 *Lateral H_x field distribution at $y = 1\lambda_0$ and $y = 4.5\lambda_0$ excited by z-directed electric source at $y = 0$ inside the parallel-plate waveguide with one corrugated surface*

Hard frequency is at 10 GHz

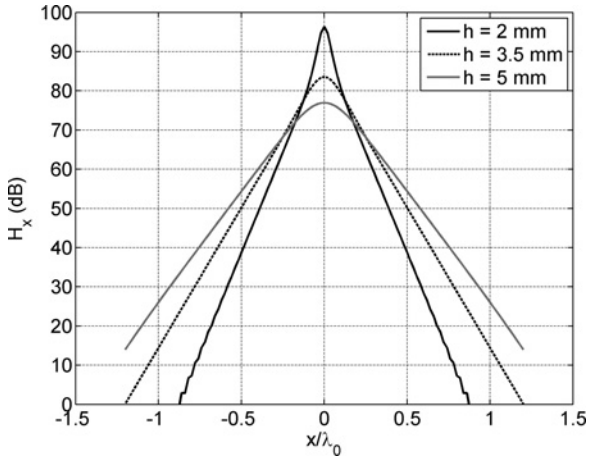

Figure 9 *Lateral H_x field distribution at $y = 4.5\lambda_0$ excited by z-directed electric source at $y = 0$ inside the parallel-plate waveguide with one corrugated surface evaluated at 10 GHz*

Parameter is the gap height h

for the following dimensions: $h = 3.5$ mm, $d = 4.33$ mm, $\varepsilon_r = 4$ and $W/P = 0.85$.

The results for two observation points are plotted in Fig. 7 as a function of frequency. One observation point is located $4.5\lambda_0$ (λ_0 is defined by hard boundary condition, (12)) away from the source in the direction along the corrugations (H_x component is plotted), and the other is located $1\lambda_0$ away from the source in the direction perpendicular to corrugations (H_y component is plotted). For comparison, the results obtained using CST Microwave Studio are also given, as already computed and presented in [9], showing good agreement.

The field distribution in the transverse plane at two distances from the source in the direction along the corrugations is presented in Fig. 8, for two frequencies. We see that the rate of the field decay away from the ridge is approximately 70 dB/λ, proving that the field is very tightly confined to the corrugations that are located just below the source. Furthermore, at the hard frequency of 10 GHz (12) there is no widening of the lateral H-field distribution along the guiding corrugations, corresponding to almost ideal 1D wave propagation. At 9.5 GHz (as well as at other nearby frequencies) the lateral H-field distribution widens slightly since the pole position in the complex plane is now a function of both the k_x and k_y variables, corresponding to a 2D wave propagation. In Fig. 9 the gap height h is chosen as a parameter, and the field distributions are evaluated at the hard frequency (10 GHz). As expected, it can be seen that when the gap height h is reduced, the lateral field distribution becomes even more confined.

To provide a rough idea concerning the quality of the local guiding properties of the waveguide with the corrugations, Tables 1 and 2 give a comparison of the lateral field decay

Table 1 *H*-field decay rate in the waveguide with corrugations as a function of waveguide height; at hard frequency $f = 10$ GHz, observation point at $y = 4.5\lambda_0$

	$h = 2$ mm	$h = 3.5$ mm	$h = 5$ mm
corrugated waveguide	103 dB/λ_0	72 dB/λ_0	53 /λ_0
ideal PEC/PMC waveguide	185 dB/λ_0	117 dB/λ_0	82 dB/λ_0

Table 2 *H*-field decay rate in the waveguide with corrugations as a function of frequency, gap height $h = 3.5$ mm, observation point at $y = 4.5\lambda_0$

	$f = 9.5$ GHz	$f = 10$ GHz	$f = 10.5$ GHz
corrugated waveguide	60 dB/λ_0	72 dB/λ_0	47 dB/λ_0
ideal PEC/PMC waveguide	116.7 dB/λ_0	116.9 dB/λ_0	117.2 dB/λ_0

rate for some waveguide gap heights and frequencies. The results show very high decay rates even when the frequency is moved from the central hard frequency and when the gap width is increased. For comparison the results for ideal PEC/PMC waveguide are also given in the tables.

4 2D periodic type structure

The spectral Green's functions for the 2D periodic type without the ridge or strip can be derived in the same way as for the 1D periodic type in Section 3, but by using the general anisotropic surface admittance introduced in Section 2.2. The result is

$$\tilde{\tilde{G}}^{\mathrm{HJ}}_{xz} = \frac{1}{\beta^2 D_{\mathrm{SW}}}\left[C_1 k_x\left(\frac{\cos k_z z}{\sin k_z h} + \frac{\sin k_z z}{\cos k_z h}\right) + C_2 k_y \frac{\cos k_z z}{\sin k_z h} + C_3 \frac{k_y}{k_z}\frac{\sin k_z z}{\sin k_z h}\right] \quad (16a)$$

$$\tilde{\tilde{G}}^{\mathrm{HJ}}_{yz} = \frac{1}{\beta^2 D_{\mathrm{SW}}}\left[C_1 k_y\left(\frac{\cos k_z z}{\sin k_z h} + \frac{\sin k_z z}{\cos k_z h}\right) - C_2 k_x \frac{\cos k_z z}{\sin k_z h} - C_3 \frac{k_x}{k_z}\frac{\sin k_z z}{\sin k_z h}\right] \quad (16b)$$

where

$$C_1 = jk_x k_y k_z(\tilde{Y}_{yx} - \tilde{Y}_{xy}) \quad (17a)$$

$$C_2 = -\beta^2 \eta_0 k_0 \tan(k_z h)\tilde{Y}_{xy}\tilde{Y}_{yx} - jk_z(k_x^2\tilde{Y}_{yx} + k_y^2\tilde{Y}_{xy}) \quad (17b)$$

$$C_3 = jk_0^2 \tan(k_z h)(k_x^2\tilde{Y}_{xy} + k_y^2\tilde{Y}_{yx}) - k_z\beta^2 \quad (17c)$$

$$D_{\mathrm{SW}} = -\tilde{Y}_{yx}(k_0^2 - k_x^2) - \tilde{Y}_{xy}(k_0^2 - k_y^2) + jk_0 k_z\left[\eta_0 \tan(k_z h)\tilde{Y}_{xy}\tilde{Y}_{yx} - \frac{1}{\eta_0}\cot(k_z h)\right] \quad (17d)$$

We will now evaluate some results for our two special cases, when the lower surface is a PMC and a bed-of-nails.

4.1 Ideal PMC

The PMC is a special case of the above general surface impedance case, giving

$$\tilde{Y}_{yx} = \tilde{Y}_{xy} = 0 \quad (18)$$

$$D_{\mathrm{SW}} = -\frac{1}{\eta_0}\cot(k_z h) \quad (19)$$

The cut-off frequency of the lowest mode is defined with $(2\pi/\lambda)h = \pi/2$, that is, there are no waveguide modes present if the gap of the waveguide is smaller than $\lambda/4$. The fields excited in such a waveguide will be discussed below, as an ideal case of the 2D periodic type of waveguide.

4.2 Bed-of-nails structure

The bed-of-nails is a very promising surface for use in gap waveguides. It is 2D periodic and can therefore exhibit cut-off property in all directions of wave propagation between the two plates. The topology of the surface is shown in Fig. 10. It consists of metallic pins attached to a ground plane, and the pins can be embedded in a dielectric medium. In practice, the dielectric is not necessary and it is actually unwanted at high frequencies due to losses, but in our analysis we shall take into account the same dielectric as in the 1D periodic case (corrugations) for comparison reasons.

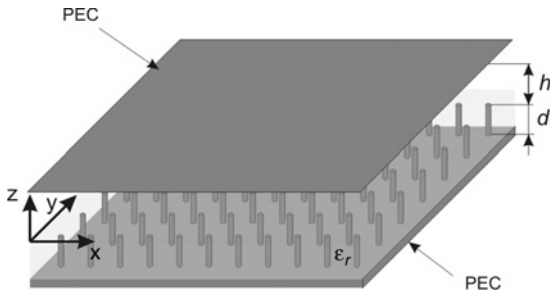

Figure 10 *Illustration of two parallel plates for use in a single-ridge/strip gap waveguide, wherein one of the plates has a high surface impedance realised by a bed-of-nails*

doi: 10.1049/iet-map.2009.0399

The homogenisation method in [3] is based on modelling the pins structure as a uniaxial medium whose permittivity may be characterised by the permittivity tensor

$$\underline{\underline{\varepsilon}} = \varepsilon_0\varepsilon_r(\hat{x}\hat{x} + \hat{y}\hat{y} + \varepsilon_{zz}(\lambda, k_z, P, r_w)\hat{z}\hat{z}) \tag{20}$$

Note that the z-component of the permittivity tensor depends on the direction of the incoming plane wave, on the periodicity of the structure P and on the radius of the wires r_w [3]. The model predicts that such a wire medium can support three different types of modes: transverse electromagnetic (TEM), transverse magnetic (TM) and transverse electric (TE) modes (relative to the direction of the pins, i.e. the z-direction). Using the TE–TM decomposition of the electric point source and by imposing the appropriate boundary conditions at all the interfaces, it is possible to obtain the reflection coefficients for both polarisations. For the TM case, the result [3] is

$$\Gamma^{TM} = -\frac{k_{die}k_p^2\tan(k_h d) - \beta^2\gamma_{TM}\tanh(\gamma_{TM}d) + \varepsilon\gamma_0(k_p^2+\beta^2)}{k_{die}k_p^2\tan(k_h d) - \beta^2\gamma_{TM}\tanh(\gamma_{TM}d) - \varepsilon\gamma_0(k_p^2+\beta^2)} \tag{21}$$

Here k_{die} is the wavenumber in the pins medium with permittivity ε_r, k_p is the plasma wavenumber of the pins lattice $(k_p^2 = 1/a^2[2\pi/(\ln(a/2\pi b) + 0.5275)])$, $\beta^2 = k_x^2 + k_y^2$, $\gamma_{TM} = \sqrt{k_p^2 + \beta^2 - k_{die}^2}$ and $\gamma_0 = \sqrt{\beta^2 - k_0^2}$. In the TE case, the electric field is perpendicular to the pins and not affected by them. Consequently, we are left only with the dielectric slab and the reflection coefficient can be found to be

$$\Gamma^{TE} = -\frac{\sqrt{k_h^2 - \beta^2} - j\sqrt{k_0^2 - \beta^2}\tan\left(d\sqrt{k_{die}^2 - \beta^2}\right)}{\sqrt{k_h^2 - \beta^2} + j\sqrt{k_0^2 - \beta^2}\tan\left(d\sqrt{k_{die}^2 - \beta^2}\right)} \tag{22}$$

The surface impedances of the bed-of-nails structure for these two polarisations are now found to be

$$\tilde{Y}_{xy}^{TM} = \tilde{Y}_{yx}^{TM} = \frac{k_0}{\eta_0 k_z}\cdot\frac{\Gamma^{TM}+1}{\Gamma^{TM}-1} \tag{23a}$$

$$\tilde{Y}_{xy}^{TE} = \tilde{Y}_{yx}^{TE} = \frac{k_z}{\eta_0 k_0}\cdot\frac{\Gamma^{TE}+1}{\Gamma^{TE}-1} \tag{23b}$$

We shall first analyse the behaviour of the surface modes appearing in the parallel-plate waveguide partly filled with the wire medium. As before, the surface waves are defined with the equation $D_{SW} = 0$. The analysed structure is similar to the one used for the corrugated case. The permittivity of the dielectric slab is 4.0 and the thickness of the bed-of-nails structure is 4.33 mm (the same as before). The period of the metallic pins is 3.75 mm and the diameter of the pins is 0.375 mm. The gap height is again 3.5 mm.

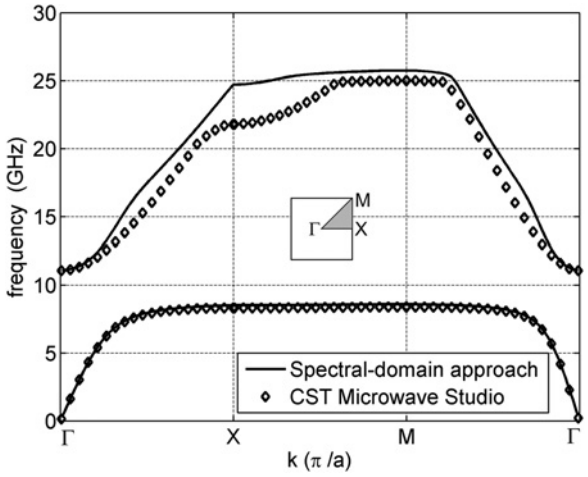

Figure 11 *Dispersion diagram for the parallel-plate waveguide with bed-of-nails structure inserted (pins are in the dielectric medium $\varepsilon_r = 4$)*

As expected, the dispersion plot in Fig. 11 shows that surface wave propagation is possible in all directions for frequencies outside the stopband which is now between 8.6 and 11.1 GHz. Using CST Microwave Studio to model the actual non-homogeneous pin surface, the predicted bandgap is between 8.4 and 11.1 GHz. The comparison of Figs. 5 and 11 gives us foundation to consider the bed-of-nails structure as a kind of 2D corrugated surface.

In the same way as for the corrugations, it is possible to derive an approximate expression for the cut-off frequencies of the waveguide partly filled with bed-of-nails. The lower cut-off frequency is the soft frequency, and the higher cut-off wavelength is approximated with the expression

$$\lambda_{cut-off} = \frac{1}{2}\pi^2\cdot b\cdot\sqrt{\varepsilon_r}\cdot\left[-1+\sqrt{1+\frac{16}{\pi^2}\frac{d}{b}}\right] \tag{24}$$

It is important to be aware that these approximations for the cut-off wavelengths are valid only asymptotically for small periods approaching zero, so they may not necessarily agree with the numerical results in [11].

Fig. 12 shows the transversal magnetic field magnitude with respect to frequency for parallel-plate waveguide shown. The observation point was located $3\lambda_0$ in x-direction and $1\lambda_0$ in y-direction away from the source point, where λ_0 is taken at the central frequency of 10 GHz. As before, the source is a short vertical dipole located below the upper waveguide plate. For comparison the results obtained using CST MW Studio are also plotted. The stopband properties of the bed-of-nails surface are clearly visible, and the results obtained by two analysis methods agree well.

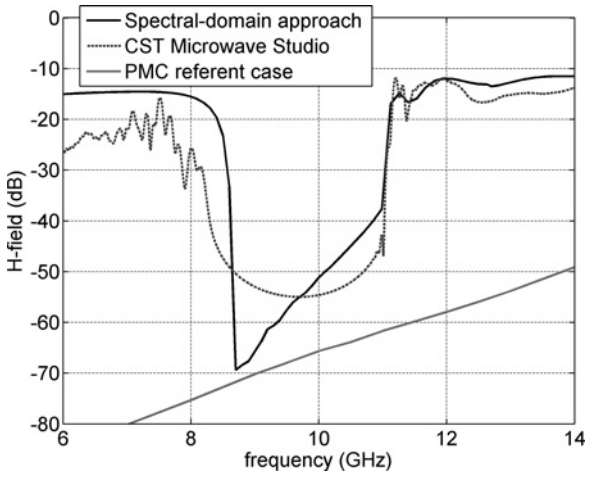

Figure 12 *Plot of the transversal magnetic field for the parallel-plate waveguide with bed-of-nails surface (the medium surrounding the pins is a dielectric with $\varepsilon_r = 4$).*

4.3 Transmission line formed by ridge or strip

The solution method for this case (depicted in Fig. 13) was described generally in Section 2.4. The computed propagation constant is compared to the result obtained using CST Microwave Studio in Fig. 14. These were computed for the actual non-homogenised geometry, with the geometrical parameters being the same as in the previous subsection with the addition of the ridge with a width of $w = 7.5$ mm. We see that the propagation coefficient of the transmission line mode is relatively close to the light line ($k_{ef}/k_0 = 1$), showing that the considered mode is a quasi-TEM mode. It is important to notice that due to the presence of the dielectric the computed propagation coefficient crosses the light line ($k_{ef}/k_0 = 1$) which would not have been the case if there was no dielectric in the pins structure.

Furthermore, Fig. 15 shows the plot of the TM field (H_y component) computed 0.5 mm above the ridge. The lateral decay for this case is approximately 70 dB/λ_0 at the central frequency of 10 GHz which is comparable with the corrugated structure. Also, the agreement with CST results is very good, except for the little offset between the curves.

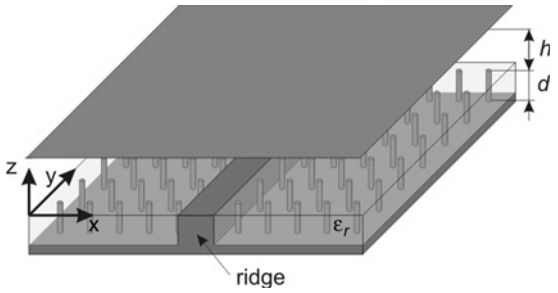

Figure 13 *Single-ridge type waveguide (the periodic texture is the pins surface)*

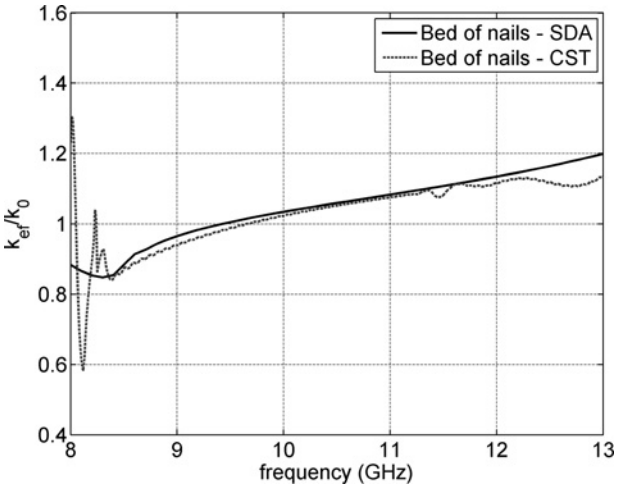

Figure 14 *Propagation constant of the fundamental mode of the example ridge gap waveguide, computed with the present method and with CST Microwave Studio*

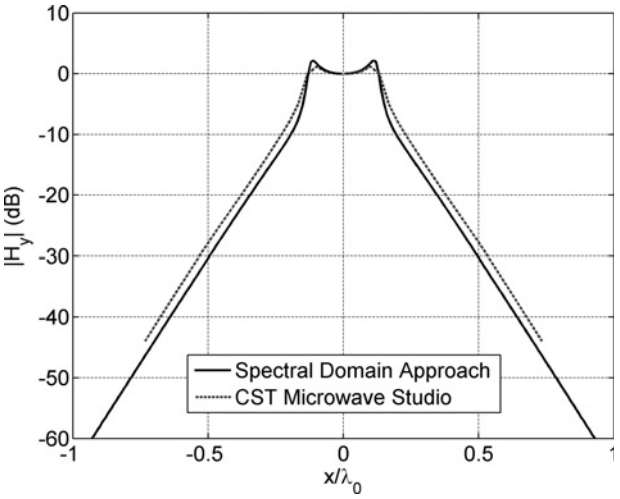

Figure 15 *Comparison between spectral-domain approach and CST Microwave Studio for the lateral H_y field distribution ($y = 3\lambda_0$ and the field is computed 0.5 mm above the ridge)*

Table 3 *H*-field lateral decay rate computed with spectral-domain approach in the single-ridge waveguide with bed-of-nails and an ideal PMC structure, as a function of waveguide height; frequency $f = 10$ GHz

	$h = 2$ mm	$h = 3.5$ mm	$h = 5$ mm
bed-of-nails structure	91 dB/λ_0	70 dB/λ_0	56 dB/λ_0
ideal PMC structure	120 dB/λ_0	92 dB/λ_0	81 dB/λ_0

This offset is expected due to the edge condition included in the assumed x-variation of the current distribution, and the omission of the transverse current components on the ridge. We first tried to use a uniform current distribution,

IET Microw. Antennas Propag., 2010, Vol. 4, Iss. 11, pp. 1799–1810

doi: 10.1049/iet-map.2009.0399

Table 4 *H*-field lateral decay rate computed with spectral-domain approach in the single-ridge waveguide with bed-of-nails and an ideal PMC structure, as a function of frequency; gap height $h = 3.5$ mm

	$f = 9.5$ GHz	$f = 10$ GHz	$f = 10.5$ GHz
bed-of-nails structure	73 dB/λ_0	70 dB/λ_0	67 dB/λ_0
ideal PMC structure	87 dB/λ_0	92 dB/λ_0	97 dB/λ_0

but then the discrepancy was larger. The present results are obtained using the edge condition of a 90° wedge, as explained in Section 2.4.

Tables 3 and 4 give a comparison of the lateral field decay rate for different gap heights and frequencies. The decay rates show that the bed-of-nails structure can also very tightly confine the field only to the guiding ridge proving excellent properties of this type of waveguides.

5 Conclusions

This paper has presented an analytical and a numerical analysis using the Green's function approach for parallel-plates with one wall replaced by a metamaterial-based periodic texture. The periodic structure is designed in such a way that the ordinary global parallel-plate modes are in cut-off, thus forcing the electromagnetic fields to propagate only along one or more guiding ridges or strips. For this reason we have performed the analysis for these different types of periodic structures: ideal PEC/PMC strip grid (i.e. an ideal soft and hard surface), longitudinal metal corrugations, an ideal PMC and a bed-of-nails (being a good representation of an isotropic artificial magnetic conductor). The two former cases have 1D periodicity in the surface, whereas the latter two have 2D periodicity.

The Green's functions were derived in the plane-wave spectral domain using homogeneous asymptotic boundary conditions. Since the poles of the obtained spectral Green's functions correspond to waveguide modes, it was possible to analyse the dispersion properties of these modes and compute the field distributions. The computed dispersion diagrams proved the existence of parallel-plate stopbands within which guiding in only one direction is allowed (1D periodic type gap waveguide), or only along the inserted guiding ridge or strip (2D periodic-type gap waveguide).

For the 1D periodic type, it was shown that the guiding of waves exists only in the direction parallel with the corrugations, and that the waves are ideally confined only at the hard frequency when the corrugations work as a PEC/PMC strip grid. Nevertheless, depending on the dimensions, we achieved very large lateral decay rates away from the guiding ridges, having values between 50 and 120 dB/λ. Furthermore, to allow simpler evaluation of the stopbands, practical expressions were derived for the lower and upper cut-off frequencies of the parallel-plate stopband in the transverse (soft) direction.

By locating a single ridge or strip within a parallel-plate structure with a 2D periodicity, we could formulate a dispersion equation in integral form by satisfying the boundary conditions on the ridge or strip. The plotted dispersion diagram revealed the presence of confined quasi-TEM mode within the stopband of the 2D periodic parallel-plate structure. The modal fields were computed showing lateral decay rates away from the guiding ridge of between 50 and 120 dB. In the same way as for the 1D periodic surface type, analytic expressions for the cut-off frequencies of the stopband were derived, valid asymptotically in the limit of vanishing period of the 2D periodic texture.

The computation of the dispersion diagram for the 2D periodic case was done by approximating the currents on the ridge to be entirely longitudinal. In reality, there may be a small asymmetric transverse component. Still, the results were in quite good agreement with solutions obtained using the general commercial CST solver. There is a need to study the current distribution further, for example, by expanding the current in a complete basis function series and by determining the coefficients using the moment method. Then, the spectral Green's functions will be needed, as presented in this paper.

The presented method and Green's functions were verified through comparison with the results obtained by a general electromagnetic solver, showing good agreement. Therefore the developed formulation of Green's functions can be used as a basis of an efficient moment method program for analysing gap waveguide circuits and antennas, in a manner similar to that for analysing microstrip structures. Consequently, this method results in a significantly increased computational efficiency compared to the general electromagnetic solvers based on FEM or FDTD methods.

6 Acknowledgment

This work has been supported partly by the Croatian Ministry of Science, Education and Sports, and partly by the Swedish Foundation for Strategic Research (SSF) within the Strategic Research Center Charmant at Chalmers.

7 References

[1] KILDAL P.-S., ALFONSO E., VALERO-NOGUEIRA A., RAJO-IGLESIAS E.: 'Local metamaterial-based waveguides in gaps between parallel metal plates', *IEEE Antennas Wirel. Propag. Lett. (AWPL)*, 2009, **8**, pp. 84–87

[2] SIEVENPIPER D., ZHANG L.J., BROAS R.F.J., ALEXOPOLOUS N.G., YABLONOVITCH E.: 'High-impedance electromagnetic surfaces

with a forbidden frequency band', *IEEE Trans. Microw. Theory Tech.*, 1999, **47**, (11), pp. 2059–2074

[3] SILVEIRINHA M.G., FERNANDES C.A., COSTA J.R.: 'Electromagnetic characterization of textured surfaces formed by metallic pins', *IEEE Trans. Antennas Propag.*, 2008, **56**, (2), pp. 405–415

[4] KILDAL P.-S.: 'Artificially soft and hard surfaces in electromagnetics', *IEEE Trans. Antennas Propag.*, 1990, **38**, (10), pp. 1537–1544

[5] KILDAL P.-S., KISHK A.: 'EM modeling of surfaces with STOP or GO characteristics – artificial magnetic conductors and soft and hard surfaces', *ACES J.*, 2003, **18**, (3), pp. 32–40

[6] NG MOU KEHN M., NANNETTI M., CUCINI A., MACI S., KILDAL P.-S.: 'Analysis of dispersion in dipole-FSS loaded hard rectangular waveguide', *IEEE Trans. Antennas Propag.*, 2006, **54**, (8), pp. 2275–2282

[7] VALERO-NOGUEIRA A., ALFONSO E., HERRANZ J.I., BAQUERO M.: 'Planar slot-array antenna fed by an oversized quasi-TEM waveguide', *Microw. Opt. Technol. Lett.*, 2007, **49**, (8), pp. 1875–1877

[8] PADILLA DE LA TORRE P., FERNÁNDEZ J.M., SIERRA-CASTAÑER M.: 'Characterization of articial magnetic conductor strips for parallel plate planar antennas', *Microw. Opt. Technol. Lett.*, 2008, **50**, (2), pp. 498–504

[9] ALFONSO E., KILDAL P.-S., VALERO A., HERRANZ J.I.: 'Detection of local quasi-TEM waves in oversized waveguides with one hard wall for killing higher order global modes'. IEEE Int. Symp. on Antennas and Propagation (IEEE AP-S), San Diego, USA, July 2008

[10] RAJO-IGLESIAS E., UZ ZAMAN A., KILDAL P.-S.: 'Parallel plate cavity mode suppression in microstrip circuit packages using a lid of nails', *IEEE Microw. Wirel. Compon. Lett.*, 2010, **20**, (1), pp. 31–33

[11] RAJO-IGLESIAS E., KILDAL P.S.: 'Numerical studies of bandwidth of parallel plate cut-off realized by bed of nails, corrugations and mushroom-type EBG for use in gap waveguides'. Submitted to IET Microwaves, Antennas and Propagation, May 2009

[12] RAJO IGLESIAS E., CAIAZZO M., INCLAN-SANCHEZ L., KILDAL P.-S.: 'Comparison of bandgaps of mushroom-type EBG surface and corrugated and strip-type soft surfaces', *IET Microw. Antennas Propag.*, 2007, **1**, (2), pp. 184–189

[13] CST Microwave Studio 2008. Available at www.cst.com

[14] POZAR D.: 'Radiation and scattering from a microstrip patch on a uniaxial substrate', *IEEE Trans. Antennas Propag.*, 1987, **35**, (6), pp. 613–621

[15] DAS N.K., POZAR D.M.: 'A generalized spectral domain Green's function for multilayer dielectric substrates with applications to multilayer transmission lines', *IEEE Trans. Microw. Theory Tech.*, 1987, **35**, (3), pp. 326–335

[16] CHEW W.C.: 'Waves and fields in inhomogeneous media' (IEEE Press, 1995)

[17] SIPUS Z., KILDAL P.-S., LEIJON R., JOHANSSON M.: 'An algorithm for calculating Green's functions of planar, circular cylindrical and spherical multilayer substrates', *Appl. Comput. Electromagn. Soc. J.*, 1998, **13**, (3), pp. 243–254

[18] KILDAL P.-S., KISHK A., SIPUS Z.: 'Asymptotic boundary conditions for strip-loaded and corrugated surfaces', *Microw. Opt. Technol. Lett.*, 1997, **14**, (2), pp. 99–101

[19] SIPUS Z., MERKEL H., KILDAL P.-S.: 'Green's functions for planar soft and hard surfaces derived by asymptotic boundary conditions', *IEE Proc. Microw. Antennas Propag.*, 1997, **144**, (10), pp. 321–328

[20] NEWMAN E.H., FORRARI D.: 'Scattering from a microstrip patch', *IEEE Trans. Antennas Propag.*, 1987, **35**, (3), pp. 245–251

[21] GOTHELF U.V., ØSTERGAARD A.: 'Full-wave analysis of a two slot microstrip filter using a new algorithm for computation of the spectral integrals', *IEEE Trans. Microw. Theory Tech.*, 1993, **41**, (1), pp. 101–108

[22] JACKSON R.W., POZAR D.M.: 'Full-wave analysis of microstrip open-end and gap discontinuities', *IEEE Trans. Microw. Theory Tech.*, 1985, **33**, (10), pp. 1036–1042

[23] JONES D.S.: 'The theory of electromagnetism' (Pergamon Press, 1964)

[24] FELSEN L.B., MARCUVITZ N.: 'Radiation and scattering of waves' (Prentice-Hall, 1973)

doi: 10.1049/iet-map.2009.0399